



HAL
open science

From neogene thin-skin to recent thick-skin deformation in Haiti fold-and-thrust belt (Western Hispaniola)

Jacques Dentzer, Manuel Pubellier, Nadine Ellouz-Zimmermann, Hildegonde Cenatus Amilcar, Heliot Amilcar, Roberte Momplaisir, Dominique Boisson

► To cite this version:

Jacques Dentzer, Manuel Pubellier, Nadine Ellouz-Zimmermann, Hildegonde Cenatus Amilcar, Heliot Amilcar, et al.. From neogene thin-skin to recent thick-skin deformation in Haiti fold-and-thrust belt (Western Hispaniola). *Journal of Structural Geology*, 2021, 151, pp.104414. 10.1016/j.jsg.2021.104414 . hal-03388674

HAL Id: hal-03388674

<https://ifp.hal.science/hal-03388674>

Submitted on 2 Aug 2023

HAL is a multi-disciplinary open access archive for the deposit and dissemination of scientific research documents, whether they are published or not. The documents may come from teaching and research institutions in France or abroad, or from public or private research centers.

L'archive ouverte pluridisciplinaire **HAL**, est destinée au dépôt et à la diffusion de documents scientifiques de niveau recherche, publiés ou non, émanant des établissements d'enseignement et de recherche français ou étrangers, des laboratoires publics ou privés.



Distributed under a Creative Commons Attribution - NonCommercial 4.0 International License

1 **From Neogene thin-skin to Recent thick-skin deformation** 2 **in Haiti Fold-and-Thrust Belt (Western Hispaniola)**

3

4 Jacques DENTZER a*, Manuel PUBELLIER a, Nadine ELLOUZ-
5 ZIMMERMANN b, Hildegonde CENATUS AMILCAR c,d, Héliot AMILCAR c,d,
6 Roberte MOMPLAISIR c, Dominique BOISSON c

7 a UMR 8538, Laboratoire de Géologie, Département de Géosciences, Ecole
8 normale supérieure, PSL Research University / CNRS, Paris, France,

9 b IFP Energies nouvelles, IFPEn Géosciences, Rueil-Malmaison, France

10 c Université d'Etat d'Haïti (UEH), Port-au-Prince, Haïti

11 d Fondation Trait-d'Union (FTU), Port-au-Prince, Haïti

12 **Keywords**

13 Fold-and-thrust belt, thin-skin to thick-skin tectonics, Neogene, North
14 Caribbean plate boundary, Haiti

15

16 **Abstract**

17 Haiti lies along the North Caribbean plate boundary, marked by two major left-
18 lateral strike-slip faults. A southwest-verging Trans-Haitian fold-and-thrust belt (FTB),

19 mostly affecting tertiary carbonate platform, developed in central Haiti between the
20 two faults, south of the Massif du Nord and the San Juan–Los Pozos Fault Zone, as
21 a result of north-south shortening. The large NW-SE antiformal Gonâve Island and
22 Ridge mark the southwest termination of the FTB as it encountered the Southern
23 Peninsula and Enriquillo-Plantain Garden Fault Zone. We show that this collision
24 resulted in a tightening of the deformed wedge and thrust faults rooted deeper into
25 the crust, leading to a transition from thin-skinned to thick-skinned tectonics in the
26 Pliocene. These short- (3–6 km) and long- (15–30 km) wavelength folding
27 deformations are temporally distinct in the north and more concomitant in the south,
28 where compressional thin-skinned deformation is still active. The thick-skinned
29 shortening was mostly expressed during the Quaternary, as shown by the formation
30 of folds and uplift of terraces between 1.7 Ma and today. This thick-skinned
31 detachment is characterized by a stronger imprint of strike-slip component, dragging
32 the FTB to a more E-W direction in its northwest and southeast extremities.
33 Understanding of the fault zone geometry of the recent 2010 Haiti earthquake
34 (M=7.2) could be reconsidered in the light of this tectonic transition.

35 **1. Introduction**

36 Subduction-collision transition is an important topic of scientific debate in many
37 places around the world, leading to a better understanding of the important
38 parameters involved. As plate convergence is in most cases oblique, the subduction-
39 collision transition is associated with redistribution of both the convergent front and
40 accompanying strike-slip faults, thus forming a partitioned system. Many examples of
41 extremely oblique settings have been described, for example in Southeast Asia, such
42 as in the southern Philippines or eastern Indonesia (Barrier et al., 1991; McCaffrey,

43 1996), but also in the Caribbean where, for example, the south plate boundary is
44 concerned (e.g. Escalona and Mann, 2011). In addition, typical accretionary prisms
45 are usually well documented in the oceanic domain, where they affect deep oceanic
46 sediments (Wakita, 2000), but their continuation onshore is often difficult to
47 characterise.

48 The island of Hispaniola is, therefore, a relevant example for this topic (Fig.
49 1a). Western Hispaniola (Haiti) corresponds to a recent microplate, dragged along
50 the North Caribbean Plate boundary, that docked against the North Caribbean Arc
51 (Calais et al., 1992; Mann et al., 1995, 2002; Calais et al., 2002; Rodríguez-
52 Zurrunero et al., 2020). Haiti is marked by two major left-lateral strike-slip faults: the
53 Oriente-Septentrional Fault Zone (OSFZ) and the Enriquillo-Plantain Garden Fault
54 Zone (EPGFZ) (Fig. 1b). The present day tectonic setting is, notably, dominated by
55 these two very active strike-slip faults (12 January 2010 Haiti earthquake in the
56 Southern Peninsula; $M=7.2$; Fig. 1b (e.g. Bilham, 2010)) and by a component of
57 north-south shortening (Mann et al., 1984; Calais and De Lépinay, 1993; Mann et al.,
58 2002), to the front of the main Los Pozos-San Juan Fault Zone (LPSJFZ) which
59 constitutes the backstop of the Hispaniola FTB (e.g. Possee et al., 2019).

60 In the south of eastern Hispaniola (Dominican Republic), the offshore Muertos
61 thrust belt (Byrne et al., 1985; Granja Bruña et al., 2009; Gorosabel Araus et al.,
62 2020) evolves laterally onshore to an imbricate system of carbonate platform slices,
63 thereby creating a fold-and-thrust belt (FTB) in the centre of Hispaniola composed of
64 a southwest-verging, forward propagating thrust system (Pubellier et al., 2000;
65 Hernaiz Huerta and Pérez-Estaún, 2002; Hernaiz Huerta et al., 2007). The FTB

66 records the Late Eocene to present convergence between the Gonâve Microplate
67 and the Hispaniola-Puerto Rico Microplate (Mann et al., 1995).

68 We focus on the wedge restricted by the two large wrench systems (OSFZ
69 and EPGFZ) which accommodate a very oblique convergence (Fig. 1b) (Dillon et al.,
70 1992; Mann et al., 1995; Pubellier et al., 2000). The deformation resulting from the
71 oblique convergence allows us to document the onshore propagation and
72 reactivation of structures with greater precision. The objective is therefore to better
73 understand the Eocene-to-present evolution of the structural style based on a refined
74 study of the morphology with 30-metre-resolution elevation data from the Shuttle
75 Radar Topography Mission.

76

77 Figure 1 here

78

79 Geological and morphological observations are presented from north to south,
80 in the Northwest Peninsula, the Montagnes Noires, the Matheux Range and in the
81 Gonâve Island respectively. Structural styles are thus highlighted before discussing
82 the recent geological evolution of Haiti. It is worth noting that the Massif du Nord
83 represents the internal zone and is not part of the FTB.

84 **2. The Northwest Peninsula and Montagnes Noires: two** 85 **wavelengths for two shortening events**

86 The Northwest Peninsula of Haiti is a broad area bounded to the north by the
87 Oriente-Septentrional Fault Zone (OSFZ) and to the south by a series of northwest-
88 southeast thrusts both offshore and onshore (Fig. 1b) (Leroy et al., 2015).

89 This peninsula is affected by two different wavelength ridges (Fig. 2). First, a
90 short wavelength (3 km) series of tight ridges with N140° to N150° trends is present
91 in the centre of the peninsula (a, b, c, d, e in Fig. 2b). Second, long wavelength
92 ridges (15–20 km) trending N90° to N120° mark the shape of the peninsula. Two
93 broad ridges of over 20 km in width are indeed located to the western end of the
94 Northwest Peninsula (A, B in Fig. 2b). One large ridge is west plunging (A in Fig. 2b),
95 another runs along the southwest coast (B in Fig. 2b). The latter (B in Fig. 2b) is
96 partly collapsed to the southwest with mass wasting along the shore, suggesting that
97 erosion is greater on the southern short limb of the ridge. The bathymetry shows the
98 southern part of this ridge except the small area, for which there is no data (Fig. 1b
99 and Fig. 2b).

100 The long wavelength ridges are capped by large reefal terraces (Dodge et al.,
101 1983; Mann et al., 1995; Dumas et al., 2006). These clearly drape and therefore
102 follow the overall shape of the long wavelength ridges (orange lines in Fig. 2b).
103 Between 14 and 28 coral terraces have been identified from sea-level to an altitude
104 of 600 m by Mann et al. (1995). The lowest terraces have been dated to ages
105 between 83 ka for the most recent and 130 ka for the oldest (Dodge et al., 1983;
106 Dumas et al., 2006). Finally, some terraces are even higher than 600 m, reaching

107 elevations up to 650 m and, locally, over 700 m (Boisson and Pubellier, 1987a).
108 Tectonic processes must be invoked to explain the presence of these high terraces
109 (Mann et al., 1995). Some of the highest reefal terraces, developed on Paleogene
110 series composed of limestone and volcanic clastics basement, tilt gently and the age
111 of this tilting may be estimated more precisely. This deformation was initiated before
112 1.7 Ma, which is the extrapolated age of the old and elevated terraces (Mann et al.,
113 1995), suggesting that the formation of the long wavelength ridges occurred circa
114 1.7 Ma. These long wavelength ridges affect Late Miocene series, whereas the short
115 wavelength ridges are pre-Early Miocene, which is the age of the regional
116 unconformity (Vila et al., 1986; Boisson and Pubellier, 1987a). We note that reefal
117 terraces are also deformed by penetrative fractures and joints (Cenatus Amilcar,
118 1997) indicating that post middle Pleistocene deformation occurred. Lastly, it is of
119 interest that late Pliocene early Pleistocene terraces also surround eastern
120 Hispaniola (Braga et al., 2012).

121 We interpret long wavelength ridges of the western end of the Northwest
122 Peninsula as two broad anticlines (A, B in Fig. 2b) separated by a valley underlining
123 the presence of a blind thrust (Fig. 2b). Indeed, we favour a thrust-controlled fold
124 (fold-bend-fold) separated by a valley where a blind thrust is located, because the
125 anticlines are of similar width and elevation. We thus exclude a roll-over anticline and
126 a normal fault. However, an alternative possibility would be that of a fault-propagation
127 fold. The lack of seismic data and the shape of the fold do not allow us to decide. The
128 two options are shown in Fig. 2c.

129 Two wavelengths for two shortening events (Phases T1 and T2) are also
130 interpreted to the southeast of the Northwest Peninsula in the Montagnes Noires (Fig.

131 1b). First, the progressive stacking of sedimentary units of the FTB (T1) began in
132 Early Miocene times in the Montagnes Noires and predates the deformation stage in
133 the Matheux Range (Section 3) (Pubellier et al., 2000). This deformation is expressed
134 as thrusts, which were later folded as an antiformal stack, and in some places,
135 reactivated by out-of-sequence faults during Miocene times (Desreumaux, 1985).
136 Second, a chain of narrow flatirons around the Montagnes Noires, particularly along
137 the northern flank, underlines a long wavelength reactivation (T2); this is also
138 observed around the Matheux Range (Section 3) (Fig. 1b and Fig. 3).

139

140 Figure 2 here

141

142 **3. The Matheux Range: a transition**

143 The Matheux Range – which exposes mainly Cenozoic sediments, except for
144 a very small area where the range is deeply incised to the west (Vila et al., 1988) – is
145 a large NW-SE anticlinorium (Fig. 1b and Fig. 3) (Boisson and Bien-aimé Momplaisir,
146 1987; Boisson and Pubellier, 1987b). This roughly NW-SE structure is asymmetric,
147 with a south-western vergence.

148 The morphology of the Matheux Range shows that it is in fact composed of
149 several shorter wavelength folds (a, b, c in Fig. 3c) located from the north-eastern
150 part of the Matheux Range (a in Fig. 3c) to the south-western part, along the coast (c
151 in Fig. 3c). The orientations of these short and long wavelength folds are more
152 colinear than those from the Northwest Peninsula.

153 However, extremities of the Matheux Range bend to acquire an E-W direction
154 (Fig. 1b and Fig. 3). To the southeast, the Matheux Range exhibits a virgation in the
155 E-W direction along the Cul-de-Sac Plain (Fig. 1b and Fig. 3). To the northwest, the
156 north-eastern fold bends to also acquire an E-W direction (Fig. 1b and Fig. 3). The E-
157 W bending is as well emphasised by Quaternary coral limestone terraces that form a
158 semi-circular outcrop at Saint-Marc (Fig. 3b and SM in Fig. 3c) (Mann et al., 1995). It
159 is of interest that acquisition of bathymetric and seismic data in 2012 (Leroy et al.,
160 2015) also indicates an offshore E-W structure extending the broad anticline
161 (Corbeau et al., 2016) (Fig. 1b). This E-W structure is marked by several NW-SE
162 overlapping folds, which suggest a transpressional component (Ellouz-Zimmermann
163 et al., 2017) (Fig. 1b).

164 We interpret the Matheux Range as resulting from an early short-wavelength
165 folding (Phase T1) reactivated by a long wavelength folding (Phase T2). The short
166 wavelength folds (a, b, c in Fig. 3c) of Tortonian age (T1) (Pubellier et al., 2000;
167 Wessels, 2018) were indeed re-deformed during the second phase of post late
168 Miocene shortening (Wessels, 2018). We attribute the T2 shortening to Pliocene and
169 Pleistocene age. For example, the north-eastern fold of phase T1 (a in Fig. 3c) was
170 ultimately thrust above the south-western ones (b and c in Fig. 3c) during the past
171 2 Ma. This results in a virgation of the north-eastern fold (a in Fig. 3c) which is coeval
172 with the long wavelength uplift (T2), as illustrated by the building of the reef terraces
173 (Fig. 3). As noted earlier, this long wavelength folding (T2) is more E-W oriented and
174 is associated with a left-lateral strike-slip component (Pubellier et al., 2000) and
175 occasional small NE-SW folds (Wessels, 2018).

176 Many of the faults of the Matheux Range are inherited from previous
177 deformation stages and were reactivated during these two shortening phases (T1
178 and T2). The short wavelength folds (T1) are bounded by N120° reverse and strike-
179 slip “Trans-Haitian” faults (blue faults in figures) parallel to the central Haitian FTB
180 (Boisson et al., 2005). These folds are also segmented by NE-SW faults (green faults
181 in figures) compatible with lateral ramps during the short-wavelength folding (T1).
182 Then, the recent movement along these NE-SW faults is an extensive dip-slip
183 motion, probably occurring during the long wavelength folding (T2) (Pubellier et al.,
184 1991). Some of these faults bound flatter areas, in particular in the southeast of the
185 Matheux Range in Haiti, such as in the Morne La Vigie area (MV in Fig. 3c). This was
186 interpreted as a kind of pull-apart depression (Pubellier et al., 1991), characterised by
187 the occurrence of Quaternary volcanics.

188 Lastly, the geometry of the decollement level of the Matheux Range may be
189 discussed (Wessels, 2018). The wavelengths deduced from the morphology suggest
190 a shallow decollement at around 2–3 km and a deeper one around 6–7 km. These
191 orders of decollement depth are also suggested by Wessels (2018).

192

193 Figure 3 here

194

195 **4. The Gonâve Island and Gonâve Ridge: a single Pliocene-** 196 **Quaternary event?**

197 The Gonâve Island (Butterlin, 1960; Mercier de Lépinay et al., 1985; Bien-
198 aimé Momplaisir et al., 1987; Boisson and Bien-aimé Momplaisir, 1987) is part of a
199 large offshore anticlinorium in the southwest of the Matheux Range (Fig. 1b).
200 Offshore multi-beam surveys show the continuation to the west of the large and
201 smooth “antiform” ridge (Fig. 1b) (Ellouz-Zimmermann et al., 2013). The island,
202 together with the Gonâve Ridge, represents a broad NW-SE trending ridge in the
203 middle of the Gonâve Gulf (Fig. 1b). This anticlinorium is mostly submarine, as
204 illustrated by a NNE-SSW seismic line oriented a few kilometres from the Gonâve
205 Island in the northwest direction (Fig. 4) (Ellouz-Zimmermann et al., 2013) .

206 As illustrated by the seismic line (Fig. 4b), the Gonâve Ridge is characterised
207 by two deformation stages with two different wavelengths, implying different fault
208 rooting at depth. First, short wavelength anticlines have developed, affecting a
209 sedimentary sequence situated below the blue “unconformity” limit (Fig. 4c). A
210 sequence between the blue and red/pink limits rests unconformably on top of it and
211 corresponds to a new onset of sedimentation. However, the red, pink, and yellow
212 strata overlying the blue dashed line are deformed at least locally with short
213 wavelength. Thus, the T1 deformation is also clearly post unconformity. Second, a
214 final large-scale anticline has developed more recently, deforming the whole
215 sedimentary pile. A younger sequence also caps the entire structure. Lastly, although
216 it is observed on an actively buckling seabed, no terraces are observed because the
217 large-scale anticline remains too deep underwater (Fig. 4c).

218

219 Figure 4 here

220

221 Although one can identify two shortening events on the seismic line, it is more
222 difficult to unravel them precisely from the surface morphology (Fig. 5). The surface
223 of the Gonâve Island culminates at around 775 m and 365 m above sea level in the
224 southeastern and northwestern ends respectively (Fig. 1b and Fig. 5). To the
225 southeast end of the Gônave Island, the fold is oriented E-W and is therefore parallel
226 to the EPGFZ. This southeast massif exhibits flatirons that emphasise the fold and its
227 curvature (Fig. 5b). It is sealed unconformably by Late Miocene strata (Mercier de
228 Lépinay et al., 1985; Boisson and Pubellier, 1987a). The NE-SW faults (green faults
229 on Fig. 5c) in this southeast end may be inherited from strike-slip lateral ramps of the
230 first shortening phase, possibly guided by basement inherited trends. These NE-SW
231 faults constitute a system of “piano key” faults. They accommodate relative vertical
232 offset between the thrust blocks of T1 (Fig. 5). Interestingly, a shoal is observed close
233 to the southeast end of the emerged ridge of the Gonâve Island (Fig. 3). Its
234 orientation is similar to the NE-SW faults in the Matheux Range (Fig. 3). To the
235 northwest end of the island, we suspect that Pliocene series appear as “ghosts” of
236 the bedding traces on the refined digital terrain model (DTM) (Fig. 5a). In addition, 7–
237 14 coral limestone terraces currently cover this extremity of the island (Mann et al.,
238 1995).

239 Lastly, the Gonâve Island is globally asymmetrical, as illustrated by three
240 topographic cross-sections across the island (Fig. 5). Several traces of coastal

241 landslides are observed on the shorter southwest flank of the island. As a result of
242 this late doming, “extrados” fractures also appeared to the southeast and northwest
243 ends of the island, which are possible reactivated bedding traces within Late Miocene
244 to Pleistocene series (Fig. 5).

245

246 Figure 5 here

247

248 Geomorphology combined with seismic observations allows us to propose that
249 the Gonâve Island together with the Gonâve Ridge is the morphologically
250 southernmost tectonic unit of the FTB (Fig. 1b). The propagation of deformation of
251 the FTB results from a progressive stacking of units from northeast to southwest from
252 the Early Miocene to the present (Pubellier et al., 2000). Thus, the Matheux Range
253 and the Sierra de Neiba (Dominican Republic) are young stacked units of T1
254 reformed in a transpressional environment (Pubellier et al., 2000; Hernaiz Huerta
255 and Pérez-Estaún, 2002). Similarly, the Gonâve Island and the Gonâve Ridge
256 developed southwest of the Matheux Range and form the youngest frontal unit of the
257 FTB. As described earlier, the two highest points of the Gonâve Island are a mild
258 expression of rapidly reactivated T1 deformation structures in a broad anticline
259 formed during T2.

260 We propose several steps for evolution of the Gonâve Island evolution during its
261 late uplift stage from T1 to T2 (Fig. 6):

262 - T1 Phase – (Fig. 6, top)

263 ○ Firstly, an early expression of the Gonâve Island formation, restricted to
264 its southeast end (Fig. 6, top), existed at the present-day highest part of
265 the island. Offshore, this deformation is marked by short wavelength
266 folds (Fig.4).

267 - T2 Phase – Figure 6 middle and bottom

268 ○ Secondly, beginning of phase T2, (Fig. 6, middle), the island emerged
269 gradually with a “peanut-shape”. The southeast part of the Gonâve
270 Island was already partially emerged, as indicated by the erosion of the
271 former terraces. Most of the current northwest end of the island was still
272 partly submerged and/or approaching the sea level as reefal terraces
273 were fringing in places.

274 ○ Thirdly, the two main present-day island reliefs emerged. Reef terraces
275 were still forming around the north-western end but also between the
276 two paleo-islands, resulting in an ovoid shape of the Gonâve Island.

277

278 ○ Lastly (Fig. 6, bottom), the more than 30km wide anticline continued to
279 grow and emerge as an asymmetrical one, overriding either a blind-
280 inverted structure or a deep-rooted thrust fault involving the basement.

281

282 ○ Figure 6 here

283

284 Finally, further south, the Gonâve Island and Gonâve Ridge form a
285 compressive northern margin of the Jeremie basin (Fig.1). Further southeast of the
286 Gonâve Island, active folds in the Cul-de-Sac Plain, particularly present near the
287 Azuei Lake, may correspond to the extension of a complex unit composed of the
288 Matheux Range and Gonâve Island (Fig. 1b and Fig. 7). However, in the south of the
289 Cul-de-Sac Plain, a series of overlapping tight folds probably also accommodate the
290 strike-slip motion of the EPGFZ (Fig. 1b and Fig. 7 in Cul-de-Sac Plain and around
291 Azuei Lake) (Saint Fleur et al., 2015).

292

293 Figure 7 here

294

295 **5. Discussion**

296 The analysis of geological and geomorphological data suggests two
297 successive events: an early thin-skin Phase, T1, and a late thick-skin Phase, T2,
298 (Fig. 7 and Fig. 8).

299 During the thin-skin Phase T1, deformation passed laterally from the eastern
300 Muertos thrust belt offshore of the southern Dominican Republic (Granja Bruña et al.,
301 2009, 2014; Gorosabel Araus et al., 2020) to a fold-and-thrust-belt (FTB) onshore
302 Haiti (Fig. 8, top, Phase 1). Granja-Bruña et al. (2014) suggested that this transition is
303 complex due to the indenting of the Beata ridge. The Beata ridge indenter modified
304 the distribution of decollement levels, thus implying a progressive blocking and
305 stacking of the deformation. Hernaiz Huerta and Pérez-Estaún (2002) place this

306 episode during the early Miocene, although an early Pliocene age was previously
307 assigned (Vila et al., 1990).

308 The propagation of the thin-skin deformation in Haiti is consistent with a
309 forward stacking of sedimentary units from northeast to southwest in the FTB
310 (Pubellier et al., 2000). The thin-skin phase is characterised by a short wavelength
311 (3–6 km), suggesting structures above a decollement level at a depth of 3 to 6 km in
312 the Matheux Range. This decollement level deepens towards the northeast (Fig. 7).
313 The T1 Phase, described on the basis of stratigraphy, was progressive and long-
314 lasting. It develops in Haiti from the Lower Miocene in the north to the Late
315 Miocene/Pliocene in the south.

316 As the south-westward propagating FTB reached the Southern Peninsula and
317 the EPGFZ, the collision resulted in a deeper decollement level producing a global
318 tightening of the whole wedge (Fig. 8, bottom, Phase 2). This would have triggered a
319 broader contraction and thrust faults rooted deeper into the crust for Phase T2:
320 between 15 to 30 km, increasing toward the south (Fig. 8). This change of
321 deformation could be a transition from thin-skinned to thick-skinned tectonics,
322 illustrated by the shift from short wavelength to long wavelength of the FTB. The
323 deformation is characterised by long wavelength (15–30 km) thick-skin structures and
324 is more N-S oriented. Phase T2 is recent and rapid, since it was initiated during the
325 Pliocene. This is shown, for example, by the formation and uplift of the terraces
326 between 1.7 Ma and today in the Northwest Peninsula. Thus, Phase T1 and Phase
327 T2 are well separated in the north but are almost concomitant in the south.

328 It is worth noting that use of the term “thick skin” here means that the
329 decollement responsible for large wavelength structure is necessarily rooted deeply

330 in the crust, resulting in localised tectonic inversion of pre-existing foreland basement
331 structures (Ellouz-Zimmermann et al., 2017). We propose that crustal detachment
332 should be rooted at least around 25–30km depth to explain the width of the Gonâve
333 anticlinorium. It therefore reactivated locally the basement inherited structures. This
334 suggest a decollement between the Massif du Nord and the Matheux front deeper
335 than that of Corbeau et al. (2016).

336 Currently, the Gonâve Island could mark the front of the FTB to the south. To
337 the west, the front of the FTB would migrate in the direction of the Gonâve Ridge
338 toward the southwest (Fig. 1b), inducing the progressive closure of the Jeremie
339 basin. To the east of the Gonâve Island, folds are active and combine the front of the
340 FTB and the strike-slip related echelon faults in Cul-de-Sac Plain and around Azuei
341 Lake (Fig. 1b).

342 The E-W bend of the extremities of the FTB during Phase T2 needs to be
343 further investigated in the light of the main strike-slip fault-zones and/or inherited
344 basement heterogeneities. The Phase T2 suffers the imprint of the strike-slip fault
345 movements (OSFZ in the north and EPGFZ in the south), which induced the dredging
346 of the FTB to a more E-W direction in both the northwestern and southeastern
347 extremities. It is illustrated by the virgation of the tips of the anticlines described
348 above in the Northwest Peninsula (Section 2) and Cul-de-Sac Plain (Sections 3 and
349 4).

350 Lastly, understanding of the recent 2010 Haiti earthquake (M=7.2) fault zone
351 geometry (Fig. 1b, red star) could be reconsidered in the light of this transition from
352 thin-skin to thick-skin tectonics. As noted earlier, the compressional wedge
353 encroached only recently on the Southern Peninsula and the thick-skin broad

354 anticlines are bent by the E-W strike-slip fault systems. The earthquake was located
355 (Fig. 1b, red star) at the junction with the youngest front of the wedge where thin-skin
356 and thick-skin deformations are combined, obscuring the geometry of the seismically
357 active EPGF (Fig. 1b).

358 To conclude, this study shows that geomorphology can be useful in
359 unravelling discrete tectonic events. Different wavelengths may reflect different
360 phases with different detachment depths. Here, we interpret the thin-skin
361 sedimentary wedge as an onland prolongation of the Muertos thrust belt. Later, in the
362 final stages of shortening, it passes to a thick-skin detachment, combined possibly
363 with tectonic inversion, and coupled with a stronger imprint of strike-slip component.
364 Such examples have been documented in recent convergence settings such as in
365 West Papua or Timor (Sapin et al., 2009).

366

367 Figure 8 here

368

369 **Figure Captions**

370 Fig. 1. Simplified regional structural map of western Hispaniola : a)
371 Geodynamic setting of Hispaniola (Wessels et al., 2019). b) Simplified regional
372 structural map (SRTM onshore and bathymetry offshore) between the two
373 lithospheric wrench faults: Oriente-Septentrional Fault Zone (OSFZ), Enriquillo-
374 Plantain Garden Fault Zone (EPGFZ) (Leroy et al., 2015; Bien-aimé Momplaisir et al.,
375 1987; Boisson and Bien-aimé Momplaisir, 1987; Boisson and Pubellier, 1987b,

376 1987a). Seismic line (Fig. 4). Cross-section (Fig. 7). Legend to be used for the other
377 figures.

378

379 Fig. 2. The Northwest Peninsula: (a) 1/250.000 geological map (Boisson and
380 Pubellier, 1987a); (b) SRTM topographic data and geological interpretations; (c)
381 interpreted cross-section of the Northwest Peninsula. See Fig. 1 for legend. See
382 Section 2 for A, B and a,b,c,d,e. See Supplementary material for the legend of the
383 geological map (Bien-aimé Momplaisir et al., 1987; Boisson and Bien-aimé
384 Momplaisir, 1987; Boisson and Pubellier, 1987a, 1987b).

385

386 Fig. 3. Matheux Range: (a) 1/250.000 geological map (Boisson and Bien-aimé
387 Momplaisir, 1987; Boisson and Pubellier, 1987b); SRTM topographic data at Saint-
388 Marc (b) and geological interpretations at large scale (c). SM is Saint-Marc and MV is
389 Morne La Vigie. See Fig. 1 for legend. See Supplementary material for the legend of
390 the geological map (Bien-aimé Momplaisir et al., 1987; Boisson and Bien-aimé
391 Momplaisir, 1987; Boisson and Pubellier, 1987a, 1987b).

392

393 Fig. 4. Offshore seismic line across the submarine Gonâve Anticlinorium: (a)
394 location, (b) seismic line and (c) enlargement of the seismic line (modified from
395 Ellouz-Zimmermann et al., 2013).

396

397 Fig. 5. The Gonâve Island: SRTM topographic data with enlargements of its
398 northwest (a) and southeast (b) ends, and geological interpretations (c), and
399 1/250.000 geological map (Bien-aimé Momplaisir et al., 1987; Boisson and Bien-aimé
400 Momplaisir, 1987) (d). See Fig. 1 for legend. See Supplementary material for the
401 legend of the geological map (Bien-aimé Momplaisir et al., 1987; Boisson and Bien-
402 aimé Momplaisir, 1987; Boisson and Pubellier, 1987a, 1987b).

403

404 Fig. 6. Simple schematic steps of evolution of the Gonâve Island during its
405 past emergence. See Fig. 1 for the legend.

406

407 Fig. 7. Schematic structural cross-section across Trans-Haitian ranges
408 showing the various wavelengths of the deformation, and the change in tectonic style
409 overtime (modified from Ellouz-Zimmermann et al. (2017), Pubellier et al. (2000) and
410 field observations).

411

412 Fig. 8. Simple schematic sketches of the Trans-Haitian Fold-and-Thrust Belt:
413 two phases of deformation from thin skin (T1) to thick skin (T2). See Fig. 1 for legend.

414

415 **Acknowledgements**

416 We thank the ENS, CNRS and IFPEN and we also acknowledge Richard J. F.
417 Wessels and two anonymous reviewers for their constructive comments.

418

419 **Declaration of competing interest**

420 This research has not received any specific grant from funding agencies in the
421 public, commercial, or not-for-profit sectors. The authors declare no competing
422 interests.

423 **Data Availability**

424 Data related to this article can be found at <http://dwtkns.com/srtm30m/>.

425

426 **References**

427 Barrier, E., Huchon, P., Aurelio, M., 1991. Philippine fault: A key for Philippine
428 kinematics. *Geology* 19, 32–35. [https://doi.org/10.1130/0091-](https://doi.org/10.1130/0091-7613(1991)019<0032:PFAKFP>2.3.CO;2)
429 [7613\(1991\)019<0032:PFAKFP>2.3.CO;2](https://doi.org/10.1130/0091-7613(1991)019<0032:PFAKFP>2.3.CO;2)

430 Bien-aimé Momplaisir, R., Amilcar, H., Murat Pierre, G., Cenatus Amilcar, H.,
431 1987. Carte Géologique d'Haïti: Feuille Sud-Ouest (Les Cayes)., scale 1/250.000,
432 CERCG IMAGEO CNRS.

433 Bilham, R., 2010. Structural geology: Invisible faults under shaky ground.
434 *Nature Geoscience* 3, 743–745. <https://doi.org/10.1038/ngeo1000>

435 Boisson, D., Bien-aimé Momplaisir, R., 1987. Carte Géologique d'Haïti: Feuille
436 Sud-Est (Port-au-Prince)., scale 1/250.000, CERCG IMAGEO CNRS.

437 Boisson, D., Prepetit, C., Saint-Jean, W., 2005. Notice explicative de la carte
438 géologique d'Haïti au 1/250000ème., Bureau des Mines et de l'Énergie (BME).

439 Boisson, D., Pubellier, M., 1987a. Carte Géologique d'Haïti: Feuille Nord-
440 Ouest (Môle Saint-Nicolas)., scale 1/250.000, CERCG IMAGEO CNRS.

441 Boisson, D., Pubellier, M., 1987b. Carte Géologique d'Haïti: Feuille Nord-Est
442 (Cap Haïtien)., scale 1/250.000, CERCG IMAGEO CNRS.

443 Braga, J.C., Diaz de Neira, A., Lasseur, E., Mediato, J., Aguirre, J., Abad, M.,
444 Hernaiz-Huerta, P.P., Monthel, J., Perez-Valera, F., Lopera, E., 2012. Pliocene-
445 Lower Pleistocene shallow-water mixed siliciclastics and carbonates (Yanigua and
446 Los Haitises formations) in eastern Hispaniola (Dominican Republic). *Sedimentary*
447 *Geology* 265, 182–194. <https://doi.org/10.1016/j.sedgeo.2012.04.007>

448 Butterlin, J., 1960. Géologie générale et régionale de la République d'Haïti,
449 Géologie générale et régionale de la république d'Haïti, Travaux et mémoires.
450 Éditions de l'IHEAL, Paris.

451 Byrne, D.B., Suarez, G., McCann, W.R., 1985. Muertos Trough subduction—
452 microplate tectonics in the northern Caribbean? *Nature* 317, 420–421.
453 <https://doi.org/10.1038/317420a0>

454 Calais, E., De Lépinay, B.M., 1993. Semiquantitative modeling of strain and
455 kinematics along the Caribbean/North America strike-slip plate boundary zone.
456 *Journal of Geophysical Research: Solid Earth* 98, 8293–8308.
457 <https://doi.org/10.1029/92JB03026>

458 Calais, E., Mazabraud, Y., Mann, P., Mattioli, G., Jansma, P., Mercier de

459 Lépinay, B., 2002. Strain partitioning and fault slip rates in the northeastern
460 Caribbean from GPS measurements. *Geophysical Research Letters* 29, 3-3–4.
461 <https://doi.org/10.1029/2002GL015397>

462 Calais, E., Mercier De Lepinay, B., Saint-Marc, P., Butterlin, J., Schaaf, A.,
463 1992. The northern Caribbean transcurrent plate boundary in Hispaniola:
464 palaeogeographic and structural evolution during the Cenozoic. *Bulletin de La*
465 *Société Géologique de France* 163, 309–324.

466 Cenatus Amilcar, H., 1997. Etude des Terrasses Marines Plio-Quaternaires et
467 de leur Substratum Eocene à Miocene dans la Presqu'île du Nord-Ouest et dans l'île
468 de la Tortue, Haïti, Grandes Antilles. PhD Thesis. Paris 11.

469 Corbeau, J., Rolandone, F., Leroy, S., Meyer, B., Mercier de Lepinay, B.,
470 Ellouz-Zimmermann, N., Momplaisir, R., 2016. How transpressive is the northern
471 Caribbean plate boundary? *Tectonics* 35, 1032–1046.
472 <https://doi.org/10.1002/2015TC003996>

473 Desreumaux, C., 1985. Haïti: Un modèle récent et actuel de système
474 compressif a effet centripète. Presented at the Géodynamique des Caraïbes,
475 Technip, Paris, 391–402.

476 Dillon, W.P., Austin, J.A., Scanlon, K.M., Terence Edgar, N., Parson, L.M.,
477 1992. Accretionary margin of north-western Hispaniola: morphology, structure and
478 development of part of the northern Caribbean plate boundary. *Marine and*
479 *Petroleum Geology* 9, 70–88. [https://doi.org/10.1016/0264-8172\(92\)90005-Y](https://doi.org/10.1016/0264-8172(92)90005-Y)

480 Dodge, R.E., Fairbanks, R.G., Benninger, L.K., Maurrasse, F., 1983.
481 Pleistocene Sea Levels from Raised Coral Reefs of Haiti. *Science* 219, 1423.

482 Dumas, B., Hoang, C.T., Raffy, J., 2006. Record of MIS 5 sea-level highstands
483 based on U/Th dated coral terraces of Haiti. *Quaternary International* 145, 106–118.
484 <https://doi.org/10.1016/j.quaint.2005.07.010>

485 Ellouz-Zimmermann, N., Hamon, Y., Deschamps, R., Battani, A., Pillot, D.,
486 Darnault, R., Vially, R., 2017. Synthèse finale des études entreprises sur le système
487 transpressif d'Haïti dans le cadre du projet collaboratif Haïti-FAILLE. Internal IFPEN
488 report No. 236267. IFPEN.

489 Ellouz-Zimmermann, N., Leroy, S.D., Momplaisir, R., Mercier de Lepinay, B.,
490 2013. From 2012 HAITI-SIS Survey: thick-skin versus thin-skin tectonics partitioned
491 along offshore strike-slip Faults-Haïti. *AGU Fall Meeting Abstracts* 23, T23E-2648.

492 Escalona, A., Mann, P., 2011. Tectonics, basin subsidence mechanisms, and
493 paleogeography of the Caribbean-South American plate boundary zone. *Marine and*
494 *Petroleum Geology*, Thematic Set on: Tectonics, Basinal Framework, and Petroleum
495 Systems of Eastern Venezuela, the Leeward Antilles, Trinidad and Tobago, and
496 Offshore Areas 28, 8–39. <https://doi.org/10.1016/j.marpetgeo.2010.01.016>

497 Gorosabel Araus, J.M., Granja Bruña, J.-L., Gallego-Mingo, A., Gómez de la
498 Peña, L., Rodríguez-Zurrunero, Á., Mas, R., Carbó-Gorosabel, A., Navarro-Comet,
499 J., 2020. New Constraints on the Tectono-Sedimentary Evolution of the offshore San
500 Pedro Basin (South-Eastern Dominican Republic): Implications for Its Hydrocarbon
501 Potential. *Geological Society, London, Special Publications* 504, SP504-2019.
502 <https://doi.org/10.1144/SP504-2019-224>

503 Granja Bruña, J.L., Carbó-Gorosabel, A., Llanes Estrada, P., Muñoz-Martín,
504 A., ten Brink, U.S., Gómez Ballesteros, M., Druet, M., Pazos, A., 2014.

505 Morphostructure at the junction between the Beata ridge and the Greater Antilles
506 island arc (offshore Hispaniola southern slope). *Tectonophysics* 618, 138–163.
507 <https://doi.org/10.1016/j.tecto.2014.02.001>

508 Granja Bruña, J.L., ten Brink, U.S., Carbó-Gorosabel, A., Muñoz-Martín, A.,
509 Gomez Ballesteros, M., 2009. Morphotectonics of the central Muertos thrust belt and
510 Muertos Trough (northeastern Caribbean). *Marine Geology* 263, 7–33.
511 <https://doi.org/10.1016/j.margeo.2009.03.010>

512 Hernaiz Huerta, P.P., Díaz de Neira, J.A., García-Senz, J., Deschamps, I.,
513 Genna, A., Nicole, N., Lopera, E., Escuder-Viruete, J., Ardévol, L.I., Pérez-Estaún,
514 A., 2007. La estructura del Suroeste de la República Dominicana: un ejemplo de
515 deformación en régimen transpresivo. *Boletín Geológico y Minero* 118, 337–357.

516 Hernaiz Huerta, P.P., Pérez-Estaún, A., 2002. Structure of the Peralta thrust
517 and fold belt, Dominican Republic. *Acta Geologica Hispanica* 37, 183–205.

518 Leroy, S., Ellouz-Zimmermann, N., Corbeau, J., Rolandone, F., Mercier de
519 Lépinay, B., Meyer, B., Momplaisir, R., Bruña, J.-L.G., Battani, A., Baurion, C., Burov,
520 E., Clouard, V., Deschamps, R., Gorini, C., Hamon, Y., Lafosse, M., Leonel, J.,
521 Pourhiet, L.L., Estrada, P.L., Loget, N., Lucazeau, F., Pillot, D., Poort, J., Tankoo,
522 K.R., Cuevas, J.-L., Alcaide, J.-F., Poix, C.J., Muñoz-Martín, A., Mitton, S.,
523 Rodriguez, Y., Schmitz, J., Seeber, L., Carbo-Gorosabel, A., Muñoz, S., 2015.
524 Segmentation and kinematics of the North America-Caribbean plate boundary
525 offshore Hispaniola. *Terra Nova* 27, 467–478. <https://doi.org/10.1111/ter.12181>

526 Mann, P., Burke, K., Matumoto, T., 1984. Neotectonics of Hispaniola: plate
527 motion, sedimentation, and seismicity at a restraining bend. *Earth and Planetary*

528 Science Letters 70, 311–324. [https://doi.org/10.1016/0012-821X\(84\)90016-5](https://doi.org/10.1016/0012-821X(84)90016-5)

529 Mann, P., Calais, E., Ruegg, J.C., DeMets, C., Jansma, P.E., Mattioli, G.S.,
530 2002. Oblique collision in the northeastern Caribbean from GPS measurements and
531 geological observations. *Tectonics* 21, 1057. <https://doi.org/10.1029/2001TC001304>

532 Mann, P., Taylor, F.W., Edwards, R.L., Ku, T.-L., 1995. Actively evolving
533 microplate formation by oblique collision and sideways motion along strike-slip faults:
534 An example from the northeastern Caribbean plate margin. *Tectonophysics* 246, 1–
535 69. [https://doi.org/10.1016/0040-1951\(94\)00268-E](https://doi.org/10.1016/0040-1951(94)00268-E)

536 McCaffrey, R., 1996. Slip partitioning at convergent plate boundaries of SE
537 Asia. Geological Society Special Publication, Geological Society Special Publication
538 106, 3–18. <https://doi.org/10.1144/GSL.SP.1996.106.01.02>

539 Mercier de Lépinay, B., Rebillard, P., Chorowicz, J., Letouzey, P., Vila, J.M.,
540 1985. Interprétation structurale de l'île de la Gonâve (République d'Haïti) à partir
541 d'images spatiales LANDSAT-MSS et SEASAT-SAR. In: A. Mascle (Editor),
542 Géodynamique des Caraïbes., Technip. ed. Paris.

543 Possee, D., Keir, D., Harmon, N., Rychert, C., Rolandone, F., Leroy, S.,
544 Corbeau, J., Stuart, G., Calais, E., Illsley-Kemp, F., Boisson, D., Momplaisir, R.,
545 Prépetit, C., 2019. The Tectonics and Active Faulting of Haiti from Seismicity and
546 Tomography. *Tectonics* 38, 1138–1155. <https://doi.org/10.1029/2018TC005364>

547 Pubellier, M., Mauffret, A., Leroy, S., Vila, J.-M., Amilcar, H., 2000. Plate
548 boundary readjustment in oblique convergence: Example of the Neogene of
549 Hispaniola, Greater Antilles. *Tectonics* 19, 630–648.
550 <https://doi.org/10.1029/2000TC900007>

551 Pubellier, M., Vila, J.M., Boisson, D., 1991. North Caribbean neotectonic
552 events; the Trans-Haitian fault system; Tertiary record of an oblique transcurrent
553 shear zone uplifted in Hispaniola. *Tectonophysics* 194, 217.

554 Rodríguez-Zurrunero, A., Granja-Bruña, J.L., Muñoz-Martín, A., Leroy, S., ten
555 Brink, U.S., Gorosabel-Araus, J.M., Gómez de la Peña, L., Druet, M., Carbó-
556 Gorosabel, A., 2020. Along-strike segmentation in the northern Caribbean plate
557 boundary zone (Hispaniola sector): Tectonic implications. *Tectonophysics* 776,
558 228322. <https://doi.org/10.1016/j.tecto.2020.228322>

559 Saint Fleur, N., Feuillet, N., Grandin, R., Jacques, E., Weil-Accardo, J.,
560 Klinger, Y., 2015. Seismotectonics of southern Haiti: A new faulting model for the 12
561 January 2010 M7.0 earthquake. *Geophysical Research Letters* 42, 10273–10281.
562 <https://doi.org/10.1002/2015GL065505>

563 Sapin, F., Pubellier, M., Ringenbach, J.-C., Bailly, V., 2009. Alternating thin
564 versus thick-skinned decollements, example in a fast tectonic setting: The Misool–
565 Onin–Kumawa Ridge (West Papua). *Journal of Structural Geology* 31, 444–459.
566 <https://doi.org/10.1016/j.jsg.2009.01.010>

567 Vila, J., Pubellier, M., Jeanpoix, C., Feinberg, H., Butterlin, J., Boisson, D.,
568 Amilcar, H., Amilcar, H., 1988. The Boundary Between Southern and Northern Blocks
569 of Hispaniola - Testimony to the Macaya Nappe in the Pierre-Payen Anticline (central
570 Haiti, Matheux Mountains, Greater Antilles). *Comptes rendus de l'Académie des*
571 *sciences., Série II, Mécanique, physique, chimie, sciences de l'univers, sciences de*
572 *la terre* 307, 603–608.

573 Vila, J.-M., Boisson, D., Feinberg, H., Laclède, J.M., Butterlin, J., Pubellier, M.,

574 1986. Evolution sédimentaire et structurale du bassin oligo-miocène de Trois-
575 Rivières sur la frontière décrochante nord-caraïbe (Massif du Nord d'Haïti, Grandes
576 Antilles). *Revue de Géol. Dyn. et de Géog. Phys.* 27, 35–44.

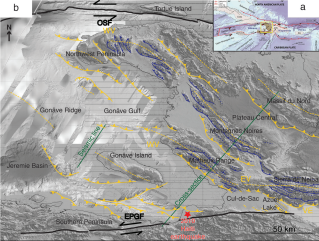
577 Vila, J.M., Jany, I., Lepvrier, C., Feinberg, H., 1990. Mise en évidence de l'âge
578 post-pliocène inférieur de la collision entre la ride de Beata et l'orogène nord-caraïbe
579 (Grandes Antilles). *C. R. Acad. Sci. Paris* 311, 1359–1366.

580 Wakita, K., 2000. Cretaceous accretionary-collision complexes in central
581 Indonesia. *Journal of Asian Earth Sciences* 18, 739–749.
582 [https://doi.org/10.1016/S1367-9120\(00\)00020-1](https://doi.org/10.1016/S1367-9120(00)00020-1)

583 Wessels, R., 2018. Tectonic evolution, fault architecture, and paleo-fluid
584 circulation in transpressive systems - southern Haiti. PhD Thesis. Sorbonne
585 Université.

586 Wessels, R.J.F., Ellouz-Zimmermann, N., Bellahsen, N., Hamon, Y.,
587 Rosenberg, C., Deschamps, R., Momplaisir, R., Boisson, D., Leroy, S., 2019.
588 Polyphase tectonic history of the Southern Peninsula, Haiti: from folding-and-
589 thrusting to transpressive strike-slip. *Tectonophysics* 751, 125–149.
590 <https://doi.org/10.1016/j.tecto.2018.12.011>

591

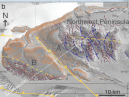
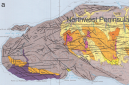


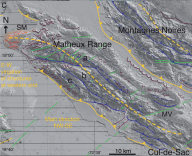
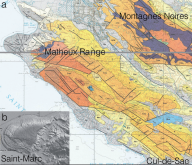
- 1st Phase (T1): Short wavelength folds
- Thrust faults and strike-slip faults
- 2nd Phase (T2): Long wavelength folds
- Thrust faults and strike-slip faults



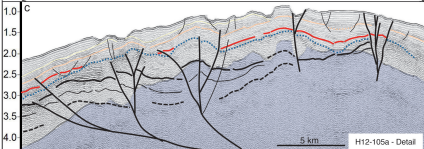
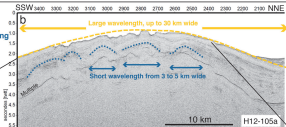
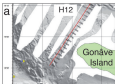
West WN, East EV
Vergences

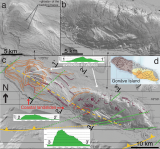
- Transfer faults (Fig. 2-4)
- Bedding traces and flatirons (Fig. 2-4)
- Terraces (Fig. 2-6)
- Scars of gravity collapse and of erosion (Fig. 2-6)



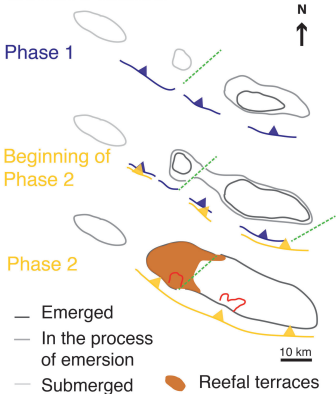


Phase T2 - Gonáve Anticlinorium
linked with extrados fracturing
Phase T1 - Initial folding & thrusting





Gonâve Island



Southern Peninsula

Trans-Haitian Range

SW

NE

EPGF



Port au Prince
(Projected)

Cul de Sac Plain

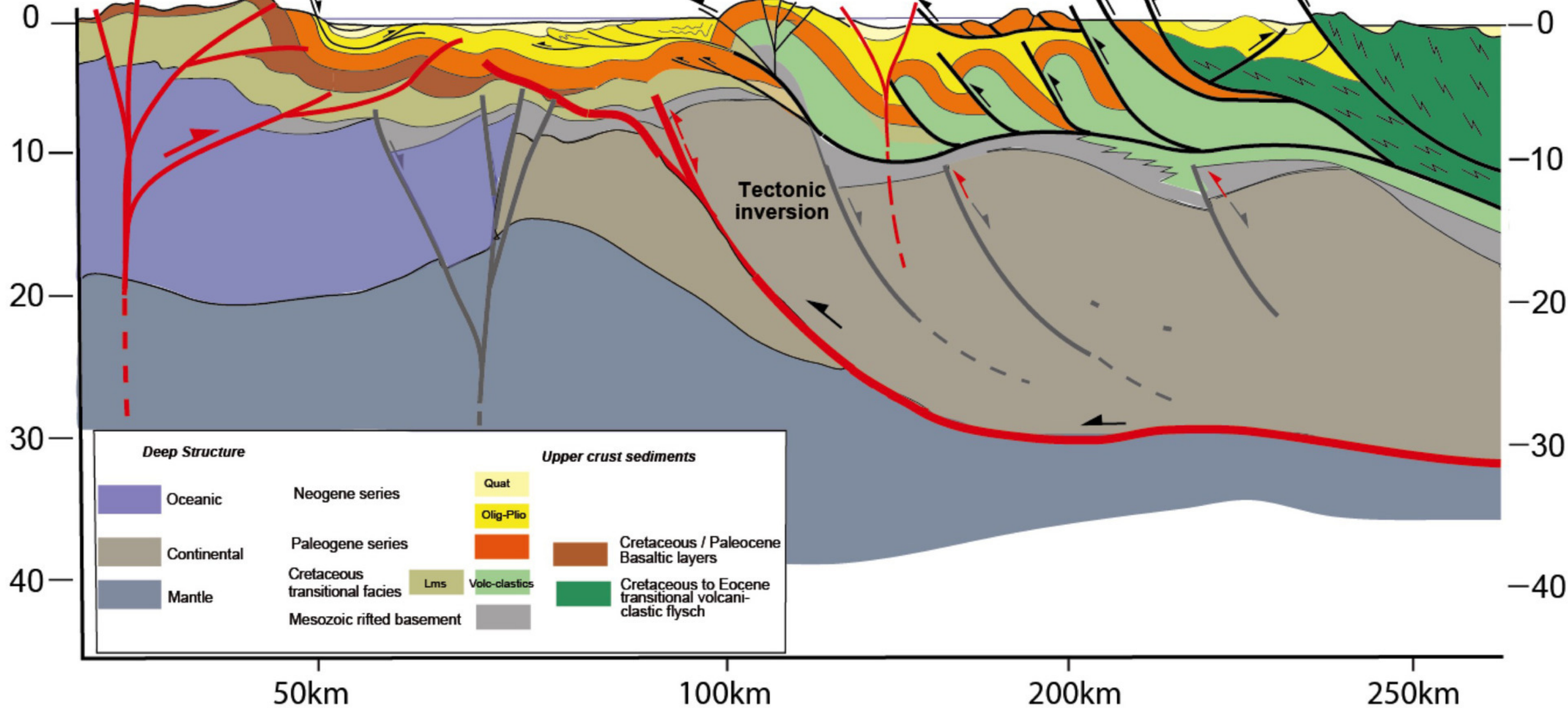
Matheux Range

Mts Noires & NW. Massif

Massif du Nord

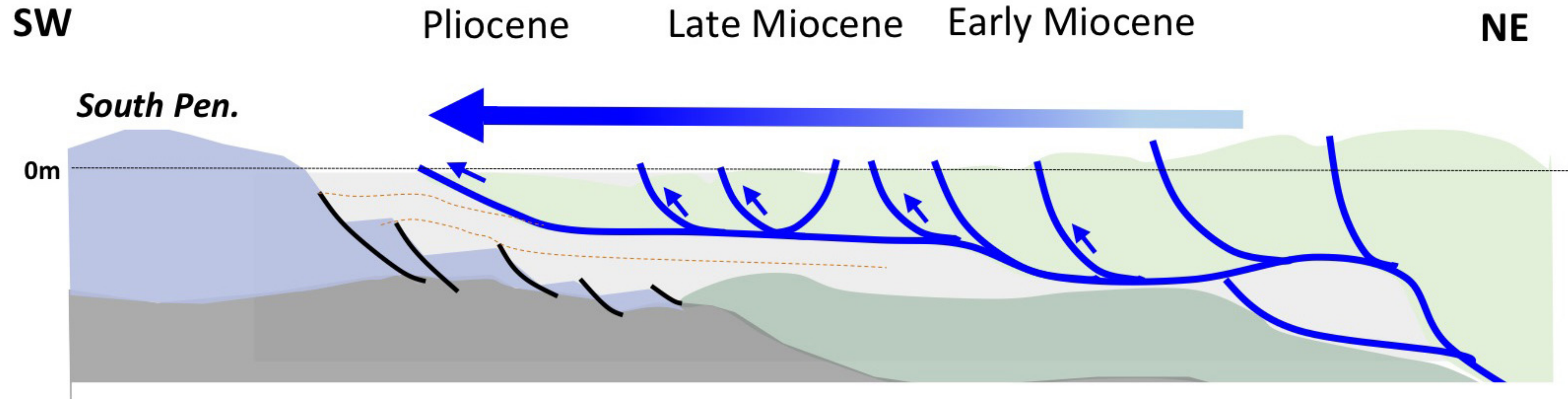
Plateau
central

LPSJ FZ



Trans-Haitian Fold-and-Thrust Belt

Phase T1



Phase T2

